Analytic estimation of subsample spatial shift using the phases of multidimensional analytic signals

A. Basarab, H. Liebgott, Philippe Delachartre

Analytic estimation of subsample spatial shift using the phases of multidimensional analytic signals

Adrian Basarab, Hervé Liebgott, Philippe Delachartre

Abstract— In this paper, a method of analytic subsample spatial shift estimation based on an a priori n-D signal model is proposed. The estimation uses the linear phases of *n* analytic signals defined with the multidimensional Hilbert transform. This estimation proposes: i) an analytic solution to the n-D shift estimation and ii) an estimation without processing complex cross-correlation function or cross-spectra between signals contrary to most phase shift estimators. The method provides better performance in estimating subsample shifts than two classical estimators, one using the maximum of cross-correlation function and the other seeking the zero of the complex correlation function phase. Two delay estimators using the in-phase and quadrature-phase components of signals are also compared to our estimator. Like most estimators using the complex signal phases, the estimator proposed herein presents the advantage of unaltered accuracy when low sampled signals are used. Moreover, we show that this method can be applied to motion tracking with ultrasound images. Thus, included in a block-based motion estimation method and tested with ultrasound data, this estimator provides an analytical solution to the translation estimation problem.

***Index Terms* – motion estimation, multidimensional analytic signal, subsample shift estimation, ultrasound imaging**

I. INTRODUCTION

SPATIAL shift estimation is applied in different fields such as sonar, radar, biomedical imaging and ultrasonics. For example, in motion estimation with block matching-based methods, shift estimation is used to locally find the shifted version of a block from one frame to the next one. This paper addresses the problem of motion tracking with ultrasound images applied to ultrasound static elastography [1], which is a technique that characterizes the elasticity of soft biological tissues.

In block matching methods, a common matching technique is to search for the shift lags that maximize or minimize cost functions such as the cross-correlation or the sum of absolute or square differences [2].

In many applications in fields such as the video or medical applications addressed in this paper, the local shifts to estimate are smaller than the image's pixel size. For video applications, different subpixel motion estimation techniques can be found in the literature, such as the quarter-pixel motion estimation of H.264 [3] or improved derivations of this method [4]. Methods based on a parabolic interpolation of the ambiguity function are also proposed; they can be used to design fine estimators for spatial shift estimation [5]. To limit the need for interpolation in subsample estimation, spatial shift estimators using the phase correlation have also been discussed in the literature [6]. A comparative study of two phase delay estimators between two noisy sinusoids is given in [7]. In this reference, a phase delay estimator using the in-phase and quadrature-phase components of the signals is proposed. This method, referred to as the unbiased quadrature delay estimator (UQDE), is an improvement on the QDE estimator proposed in [8].

For ultrasound elastography, shift estimators using the phase of the complex signals have also been proposed in [9-11] and have shown unaltered performance for low sampled signals.

Based on Jensen's work [12] and using the image formation method proposed by Liebgott et al. in [13], we can control the shape of the signals which allows us to consider an a priori signal model. This article considers an n-D signal model based on a product of n sinusoids and proposes a phase delay estimator. The estimation uses the phases of n analytic signals chosen to obtain a linear estimation problem. Moreover, these complex signals are chosen such that the linear system obtained can be analytically solved, providing an analytic estimation for our phase delay problem. The estimator is then adapted so that the relative spatial delay between two shifted versions of the proposed signal model can be estimated. We show that the proposed estimator depends less on the signal resolution than a classical estimator by maximum of correlation.

Compared to other shift estimators proposed in the literature and based on the complex signal phases, the method reported herein does not need to process the cross-correlation function between signals. The estimator is directly applied to the signals, which makes it more computer-efficient.

In section II, the signal model and the multidimensional Hilbert transforms used to generate the analytic signals are introduced. Section III describes the estimation method and the statistical behavior of the proposed estimator. Section IV shows how the estimator is used for motion tracking with a block–based motion estimation method. Sections V and VI present results on numerical simulations and experimental data. The estimator proposed is compared to the maximum of correlation estimator, an estimator based on the phase of the complex cross-correlation function and the above-mentioned QDE and UQDE estimators. Finally, conclusions are drawn in section VII.

II. SIGNAL MODEL

The problem addressed here is estimating the spatial shift parameter vector $\boldsymbol{d} = (d_1, d_2, \ldots, d_n)^T$ given the harmonic function $r : \mathbb{R}^n \to \mathbb{R}$ in (1).

.

$$r(\boldsymbol{x}) = w(\boldsymbol{x}) \prod_{k=1}^{n} cos\left(2\pi f_k \left(x_k - d_k\right)\right) \quad \textbf{(1)}$$

We denote vectors in $\mathbb{R}^n$ (n arbitrary) with boldface lowercase letters. Thus, in (1) $\boldsymbol{x} = \left(x_1, x_2, \ldots, x_n\right)^T$ denotes the n-D spatial variable, f_k are the frequencies on each direction assumed to be known and $w(\boldsymbol{x})$ is an n-D window assumed to have a disjointed Fourier spectrum from the cosinus product (see appendix for the use of the conditions on w). Notice that in this application of motion estimation, a relative shift between two signals that have the same form as in (1) will be discussed.

By analogy with the 1-D case, in the theory of the complex signal, two extensions of the Hilbert transform were defined: the total Hilbert transform [14] and the partial Hilbert transform [15]. Let us define $r_H : \mathbb{R}^n \to \mathbb{R}$ the total Hilbert transform and $r_H^p : \mathbb{R}^n \to \mathbb{R}$ the partial Hilbert transforms of r. We use small letters to denote the functions in the spatial domain and capital letters to denote their n-D Fourier transform. Let $\boldsymbol{u} = \left(u_1, u_2, \ldots, u_n\right)^T$ be the n-D frequency variable. Thus, in the Fourier domain, the Hilbert transforms are defined as follows:

$$R_H(\boldsymbol{u}) = R(\boldsymbol{u}) \prod_{k=1}^{n} \left(-j \operatorname{sign}\left(u_k\right)\right) \quad \textbf{(2)}$$

$$R_H^{\boldsymbol{p}}(\boldsymbol{u}) = R(\boldsymbol{u}) \prod_{k=1}^{n} \left(-j \operatorname{sign}\left(u_k\right)\right)^{p_k}, \quad \textbf{(3)}$$

where

$$\operatorname{sign}\left(u_k\right) = \begin{cases} 1, & if\ u_k > 0 \\ 0, & if\ u_k = 0 \\ -1, & if\ u_k < 0 \end{cases} \quad \textbf{(4)}$$

and $p_k = 1$ if the direction x_k is present in the partial Hilbert transform and $p_k = 0$ if not (p_k denotes the k^{th} element of vector $\boldsymbol{p}$). Note that the total Hilbert transform can be obtained by the partial transform if all n directions are considered. Moreover, if all vector $\boldsymbol{p}$ elements are equal to zero no Hilbert transform is processed.

Using the original function r and its Hilbert transforms introduced in (2) and (3), we can define a series of analytic signals, denoted $r_i(\boldsymbol{x})$. The analytic signals are defined in the Fourier domain by:

$$R_i(\boldsymbol{u}) = R(\boldsymbol{u}) \prod_{k=1}^{n} \left(1 + (-1)^{b_{ik}} \operatorname{sign}\left(u_k\right)\right), \quad \textbf{(5)}$$

with $1 \le i \le 2^n$. In (5) $\boldsymbol{b_i}$ represents an n-D vector whose elements can take the value of zero or one (b_{ik} denotes the k^{th} element of vector $\boldsymbol{b_i}$). Therefore, 2^n different vectors $\boldsymbol{b_i}$ and consequently 2^n analytic signals can be defined. We conclude that in the variable i is an integer between *1* and 2^n.

Example. To illustrate how the analytic signals defined in (5) are related to the Hilbert transforms introduced in (2) and (3), let us consider an example for n equal to 2 [16]. Four analytic signals can be generated in this case. Let us consider the case corresponding to $\boldsymbol{b} = (0,0)^T$, denoted r_1. Equation (5) becomes:

$$\begin{aligned} R_1(\boldsymbol{u}) &= R(\boldsymbol{u})\left(1 + \operatorname{sign}\left(u_1\right)\right)\left(1 + \operatorname{sign}\left(u_2\right)\right) \\ &= R(\boldsymbol{u})\left(1 + \operatorname{sign}\left(u_1\right) + \operatorname{sign}\left(u_2\right) + \operatorname{sign}\left(u_1\right)\operatorname{sign}\left(u_2\right)\right) \\ &= R(\boldsymbol{u}) - R_H(\boldsymbol{u}) + j\left(R_H^{\boldsymbol{p}_1}(\boldsymbol{u}) + R_H^{\boldsymbol{p}_2}(\boldsymbol{u})\right) \end{aligned} \quad \textbf{(6)}$$

with $\boldsymbol{p_1} = (1,0)^T$ and $\boldsymbol{p_2} = (0,1)^T$.

Figure 1 represents the Fourier transforms of signal r in (1) and of analytic signal r_1 calculated in (6). The example given corresponds to n equal to 2 and a Gaussian window w. We observe that the analytic signal r_1 has a single quadrant spectrum. Note that the choice of the quadrant in the Fourier domain is made by vectors $\boldsymbol{b}$.

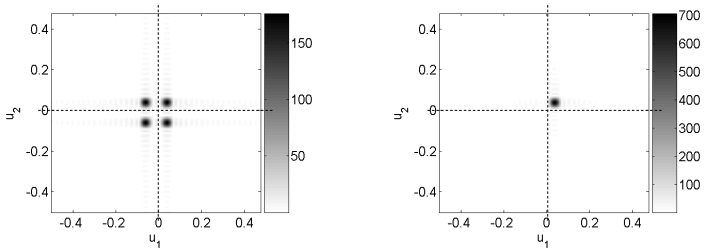

(a) (b)

Figure 1. Modulus of the 2-D Fourier transforms of (a) real signal r and (b) complex signal r_1.

For the function given in (1) and using the induction method (see appendix), we can show that the phases of the analytic signals defined previously have the form in (7).

$$\phi_i(\boldsymbol{x}) = \phi\left(r_i(\boldsymbol{x})\right) = \sum_{k=1}^{n} 2\pi f_k \left(-1\right)^{b_i(k)} \left(x_k - d_k\right) \quad \textbf{(7)}$$

III. ANALYTIC ESTIMATION

The phases of the analytic signals defined in section II are used here to estimate the n-D vector $\boldsymbol{d}$. The model of the phases in (7) leads us to consider a class of estimation problems represented by the linear model:

$$\boldsymbol{y} = H\boldsymbol{d} + \boldsymbol{v} \quad \textbf{(8)}$$

where $\boldsymbol{d}$ is the deterministic vector of unknown parameters, $\boldsymbol{y}$ is the vector containing the observations, i.e. the phases of the analytic signals, H is a known $2^n \times n$ matrix and $\boldsymbol{v}$ is the noise. This type of linear model estimation has been widely studied in the literature for the general case. Among the proposed methods, $\boldsymbol{d}$ vector is commonly estimated by searching for the vector $\hat{\boldsymbol{d}}$ so that the estimated vector $\hat{\boldsymbol{y}}$ is as close as possible to the given data $\boldsymbol{y}$. If the total squared error in the observation is used, we deal with the classical least-square (LS) estimation [17]. The LS estimation is then given by:

$$\hat{\boldsymbol{d}}_{\boldsymbol{LS}} = \left(H^T A H\right)^{-1} H^T A\, \boldsymbol{y}, \quad \textbf{(9)}$$

where A is an arbitrary positive definite weighting matrix.

It should be remembered that the purpose here is to obtain an analytic expression for the estimation of vector $\boldsymbol{d}$, i.e. which does not use a numerical algorithm to inverse the matrices in (9). Therefore, we propose to restrict to n the number of observations and consequently the number of analytic signals considered. In this way, H becomes an $n \times n$ matrix. Moreover, we choose n particular analytic signals for which the matrix H is invertible and may be analytically inverted. Note also that all positive definite matrices are invertible. In

this case, the estimation in (9) becomes:

$$\hat{\boldsymbol{d}}_{\boldsymbol{AS}} = H^{-1}A^{-1}\left(H^{T}\right)^{-1}H^{T}A\boldsymbol{y} = H^{-1}\boldsymbol{y}, \quad \textbf{(10)}$$

where the subscript AS stands for analytic shift estimation.

Based on the phase model in (7) and on the linear estimation problem in (10), let us define the observations vector $\boldsymbol{y}$ as functions of measured phases $\phi_i(\boldsymbol{x})$, denoted $\Phi_i(\boldsymbol{x})$, and the matrix H.

$$y_i = \sum_{k=1}^{n}\left(2\pi f_k(-1)^{b_i(k)}x_k\right) - \Phi_i(\boldsymbol{x}),\ \textit{for } 1 \le i \le n \quad \textbf{(11)}$$

$$H = \begin{pmatrix} 2\pi f_1(-1)^{b_{11}} & \cdots & 2\pi f_n(-1)^{b_{1n}} \\ \vdots & \vdots & \vdots \\ 2\pi f_1(-1)^{b_{n1}} & \cdots & 2\pi f_n(-1)^{b_{nn}} \end{pmatrix} \quad \textbf{(12)}$$

As explained above, n different vectors $\boldsymbol{b}$ are chosen so that the matrix H is invertible. This choice was also motivated by the fact that matrix H should be easily updated when passing from n-1 dimensions to n dimensions. Moreover, the inverted matrix of H (see **(14)**) has a simple form that facilitates its analytic multiplication by vector $\boldsymbol{y}$. The possibility retained which makes H analytically invertible for all integers n is given in

.

$$\begin{pmatrix} \boldsymbol{b_1}^T \\ \boldsymbol{b_2}^T \\ \vdots \\ \boldsymbol{b_{n-1}}^T \\ \boldsymbol{b_n}^T \end{pmatrix} = \begin{pmatrix} 0 & 0 & \cdots & 0 & 0 \\ 1 & 0 & \cdots & 0 & 0 \\ \vdots & \vdots & \vdots & \vdots & \vdots \\ 1 & 1 & \cdots & 0 & 0 \\ 1 & 1 & \cdots & 1 & 0 \end{pmatrix} \quad \textbf{(13)}$$

For this series of vectors $\boldsymbol{b_i}^{\boldsymbol{T}}$, the determinant of the matrix H is shown to be equal to $2^{n-1}\prod_{k=1}^{n}(2\pi f_k)$ and consequently different from zero for non-zero frequencies. In the case considered, the inverse of the matrix H is:

$$H^{-1} = \begin{pmatrix} \frac{1}{4\pi f_1} & -\frac{1}{4\pi f_1} & 0 & \cdots & 0 \\ 0 & \frac{1}{4\pi f_2} & -\frac{1}{4\pi f_2} & \cdots & 0 \\ \vdots & \vdots & \vdots & \vdots & \vdots \\ \frac{1}{4\pi f_n} & 0 & 0 & \cdots & \frac{1}{4\pi f_n} \end{pmatrix} \quad \textbf{(14)}$$

With these assumptions and using (10), the AS of vector $\boldsymbol{d}$ gives the following result:

$$\begin{aligned} \hat{d}_{ASi} &= x_i - \frac{1}{4\pi f_i}\left(\Phi_i(\boldsymbol{x}) - \Phi_{i+1}(\boldsymbol{x})\right),\ \ \textit{for } 1 \le i \le (n-1) \\ \hat{d}_{ASn} &= x_n - \frac{1}{4\pi f_n}\left(\Phi_n(\boldsymbol{x}) + \Phi_1(\boldsymbol{x})\right) \end{aligned} \quad \textbf{(15)}$$

The result in **(15)** is obtained considering only one observation of each phase for one given value of vector $\boldsymbol{x}$. For each phase, we propose to take into account a series of measures and to calculate the final estimation as the mean value of AS estimations in **(15)**. In this multi-measure case, let us consider the definition intervals for each direction of vector $\boldsymbol{x}$ as follows:

$$M_1 \le x_1 \le N_1, \ldots, M_n \le x_n \le N_n .$$

Consequently, the mean analytic shift (MAS) estimation becomes:

$$\begin{aligned} \hat{d}_{MASi} &= \frac{M_i + N_i}{2} - \frac{\sum_{x_1=M_1}^{N_1}\cdots\sum_{x_n=M_n}^{N_n}\left[\Phi_i(\boldsymbol{x}) - \Phi_{i+1}(\boldsymbol{x})\right]}{4\pi f_i\prod_{k=1}^{n}(N_k - M_k + 1)}, \\ &\textit{for } 1 \le i \le (n-1) \\ \hat{d}_{MASn} &= \frac{M_n + N_n}{2} - \frac{\sum_{x_1=M_1}^{N_1}\cdots\sum_{x_n=M_n}^{N_n}\left[\Phi_n(\boldsymbol{x}) + \Phi_1(\boldsymbol{x})\right]}{4\pi f_n\prod_{k=1}^{n}(N_k - M_k + 1)} \end{aligned} \quad \textbf{(16)}$$

In the following, the statistical behavior of the proposed estimator is studied. We assume that the data corresponding to signal r is observed with additive zero-mean white Gaussian noise, denoted $z(\boldsymbol{x})$ and having variance σ_z^2. Let us denote the signal-to-noise ratio corresponding to signal r with *SNR*. Note that we are interested in estimating the vector $\boldsymbol{d}$ for high *SNR* (*SNR* >> 1).

The Hilbert transform is linear and does not change the statistical properties of the noise [18]. Thus, it can easily be shown that the analytic signals r_i defined previously are observed with zero-mean complex white Gaussian additive noise, denoted $z_i(\boldsymbol{x})$. Moreover, (17) gives the relation between the variance of $z_i(\boldsymbol{x})$ and σ_z^2.

$$\sigma_{z_i}^2 = Var\left(z_i(\boldsymbol{x})\right) = 2^n\sigma_z^2 \quad \textbf{(17)}$$

It should also be noted that the real and imaginary parts of the analytic signal r_i are observed with zero-mean additive noises of variances $2^{n-1}\sigma_z^2$ [19]. The signal-to-noise ratios corresponding to r_i are equal to *SNR*.

Based on Tretter's work [20], we assume that the complex additive noise on the analytic signals can be converted into an additive phase noise with the assumption of high SNR. The noise sequence $\boldsymbol{v}$ considered in (8) is in this case white Gaussian with:

$$E(\boldsymbol{v}) = 0,\ cov(\boldsymbol{v}) = \frac{1}{2\,SNR}I_n, \quad \textbf{(18)}$$

with I_n the $n \times n$ identity matrix. The two proposed estimators $\hat{\boldsymbol{d}}_{\boldsymbol{AS}}$ and $\hat{\boldsymbol{d}}_{\boldsymbol{MAS}}$ are unbiased in these conditions of high SNR and zero-mean noise. Moreover, we can calculate the covariance matrices corresponding to each of the two estimators.

$$\begin{aligned} cov\left(\hat{\boldsymbol{d}}_{\boldsymbol{AS}}\right) &= E\left[\left(\hat{\boldsymbol{d}}_{\boldsymbol{AS}} - \boldsymbol{d}\right)\left(\hat{\boldsymbol{d}}_{\boldsymbol{AS}} - \boldsymbol{d}\right)^T\right] \\ &= E\left[H^{-1}\boldsymbol{v}\left(H^{-1}\boldsymbol{v}\right)^T\right] = E\left[H^{-1}\boldsymbol{v}\boldsymbol{v}^T\left(H^{-1}\right)^T\right] \\ &= H^{-1}\,cov(\boldsymbol{v})\left(H^{-1}\right)^T = \frac{1}{2\,SNR}\left(H^TH\right)^{-1} \end{aligned} \quad \textbf{(19)}$$

$$cov\left(\hat{\boldsymbol{d}}_{\boldsymbol{MAS}}\right) = \frac{1}{\prod_{k=1}^{n}(N_k - M_k + 1)}cov\left(\hat{\boldsymbol{d}}_{\boldsymbol{AS}}\right) \quad \textbf{(20)}$$

For both estimators and considering the linear model in (8) with Gaussian noise v the Fisher information matrices are shown to be

equal to the inverses of the covariance matrices calculated in (19) and (20) [17]. We conclude that the CRLB is achieved for both AS and MAS estimators.

IV. Application to motion estimation

The estimator described is used for estimating motion using ultrasound imaging. Thus, nonconventional ultrasound images [13] are used and shown to locally follow the signal model in (1) for n equal to 2. In the present case, a block-based estimation method is used to track motion. The MAS estimator is then used to locally estimate the 2-D block translations. It replaces cost functions as the sum of absolute or square differences or the cross-correlation [2] usually used with classical block matching methods. This method proceeds in two main steps. First, four phase images are computed using the analytic signals defined in (5) applied to the two ultrasound images. The second step consists in estimating the 2-D translations of a collection of nodes (pixels) defining a rectangular grid on the reference image. For each node, local phase blocks are extracted from the four phase images calculated previously. Note that the positions of these phase blocks in the phase images take into account the initialization technique described in [21]. Using these four local phases, the MAS estimator is used to estimate the local relative 2-D shift between the images. Before applying the formula in (16), two phase differences are calculated and positions corresponding to phase jumps are eliminated. For this, a threshold equal to π is used. This value takes into account the fact that in the present application the local shifts are considered smaller than the signals normalized half periods.

The main steps of our block-based motion estimation method using the MAS estimator are given bellow.

Data: Two unconventional ultrasound images i_1 and i_2.

Phase image computation

1) Compute four complex images i_{11}, i_{12}, i_{21}, i_{22}.

$$\begin{aligned} i_{k1}(\boldsymbol{x}) &= FFT^{-1}\{I_k(\boldsymbol{u})(1+\text{sign}(u_1))(1+\text{sign}(u_1))\} \\ i_{k2}(\boldsymbol{x}) &= FFT^{-1}\{I_k(\boldsymbol{u})(1-\text{sign}(u_1))(1+\text{sign}(u_1))\} \\ &\text{for } k=1,2 \end{aligned} \quad \textbf{(21)}$$

2) Extract the phases of the four complex images:

$$\phi_{kj}(\boldsymbol{x}) = \arg\left(i_{kj}(\boldsymbol{x})\right),\ \text{for } k=1,2 \text{ and } j=1,2 \quad \textbf{(22)}$$

Translation estimation for one node

3) For each node, execute steps 4 to 7.

4) Extract two local phases denoted $\Phi_{ri}(\boldsymbol{x})$, $i=1,2$ from phase images ϕ_{11} and ϕ_{12} and two local phases $\Phi_{si}(\boldsymbol{x})$, $i=1,2$ from phase images ϕ_{21} and ϕ_{22}.

5) Compute the phase differences:

$$\Phi_i(\boldsymbol{x}) = \Phi_{si}(\boldsymbol{x}) - \Phi_{ri}(\boldsymbol{x}),\ i=1,2, \quad \textbf{(23)}$$

6) To eliminate phase jumps, find the Ω domain for which:

$$\Omega = \{\boldsymbol{x} \mid \Phi_1(\boldsymbol{x}) < \pi \text{ and } \Phi_2(\boldsymbol{x}) < \pi\}, \quad \textbf{(24)}$$

7) Compute the translations of the current node by applying the MAS estimator in (16) using $\Phi_i(\boldsymbol{x}), \boldsymbol{x} \in \Omega$.

$$\hat{\boldsymbol{d}}_{MAS} = \begin{pmatrix} \frac{1}{4\pi f_1} \underset{\boldsymbol{x}\in\Omega}{mean}\left[\Phi_2(\boldsymbol{x}) - \Phi_1(\boldsymbol{x})\right] \\ \frac{1}{4\pi f_2} \underset{\boldsymbol{x}\in\Omega}{mean}\left[\Phi_2(\boldsymbol{x}) + \Phi_1(\boldsymbol{x})\right] \end{pmatrix} \quad \textbf{(25)}$$

Result: Dense motion field between images i_1 and i_2, computed by linear interpolation of the coarse motion field estimated in each node.

V. Computer simulation results

In this section a numerical simulation was performed to show the performance of the proposed MAS estimator compared to four estimators: a generic estimator by the maximum of the cross-correlation function [22], an ultrasound elastography oriented estimator searching for the phase root of the complex cross-correlation function [10], the QDE estimator in [8] and the UQDE estimator in [7]. Given the separable form of the signal model considered (1) and of the result of our estimator (16), a 1-D simulation is sufficient to analyze its behavior. Moreover, two different ways to apply the MAS estimator are discussed. The first is presented in section IV, where the points corresponding to phase jumps are not taken into account. The second one consists in applying the MAS estimator after unwrapping the phases of the analytic signals. The 1-D phases are unwrapped by adding multiples of 2π when absolute jumps between consecutive points are greater than π.

The generated data were:

$$r(x_1) = exp\left(-\pi\left(\frac{x_1 - d_r}{\sigma_r}\right)^2\right) cos\left(2\pi f_1 (x_1 - d_r)\right) + z_r(x_1)$$

$$s(x_1) = exp\left(-\pi\left(\frac{x_1 - d_s}{\sigma_s}\right)^2\right) cos\left(2\pi f_1 (x_1 - d_s)\right) + z_s(x_1)$$

where

$$x_1 = 1,2,...,20;\ f_1 = 0.2;\ d_r = 0.4,\ d_s = 0.6;\ \sigma_r = 20,\ \sigma_s = 20$$

and $z_r(x_1)$ and $z_s(x_1)$ are computer generated zero-mean Gaussian noises with variances $\sigma_{z_r}(x_1)$ and $\sigma_{z_s}(x_1)$, respectively. The signal-to-noise ratio (SNR) is assumed to be the same for both signals. The relative shift to estimate between signals r and s is $d_1 = d_s - d_r$.

Figure 2 presents the mean and the standard deviation values obtained with each estimator in presence of noise for different SNRs. For each SNR level, 512 estimations were processed and the mean and standard deviation values are given.

MAS, QDE, UQDE and the phase root estimators were all used with signals r and s at the initial resolution. Since the accuracy of the maximum of correlation estimator depends directly on the signals resolution, the cross-correlation function was piecewise cubic spline interpolated before the maximum detection was applied. Therefore, to obtain a sample corresponding to the shift to estimate, an interpolation by a factor of 5 was processed. However, in a practical application it is difficult to predict the interpolation factor and this type of estimation is usually biased. We can note that for low SNRs, the MAS estimator gives better results without unwrapping the phase and has similar accuracy for high SNRs. The QDE, the UQDE and the phase root estimator are roughly as accurate as the MAS estimator. On the other hand, these estimators can only be applied in 1-D. Moreover, the phase root estimator works iteratively, which increases the processing time reported to the MAS estimator by 30% when three iterations are processed.

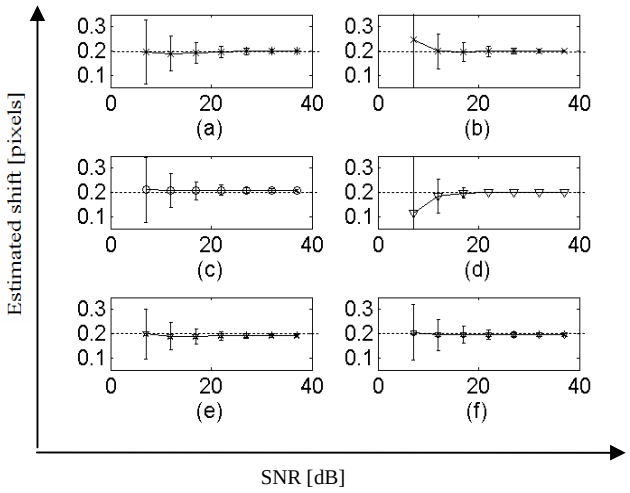

Figure 2. Shift estimation in presence of noise with (a) the MAS estimator (b) the MAS estimator using the unwrapped phase, (c) the complex correlation phase root, (d) the cross-correlation maximum, (e) the quadrature time delay estimator (QDE) and (f) the unbiased quadrature time delay estimator (UQDE). The true shift is 0.2 (dashed line).

As explained above, two possible ways to apply the MAS estimator are discussed. However, for all SNR levels considered, the domain Ω which does not include phase jumps represented at least 80% of the phase definition domain.

Figure 3 gives the behavior of the estimators versus the sampling frequency. For the same data and with an SNR of 20 dB, shift estimations were processed for signals with 3-10 samples per period. For each case, 512 estimations were processed and the mean and standard deviation values are retained. With the estimator searching for the maximum of correlation, the cross-correlation function was interpolated so that a sample corresponding to the shift to estimate was obtained. This explains why for signals with an SNR of 20 dB, the standard deviation values with this estimator are smaller than with the other methods. This estimator depends on on the shape of the signals, which explains the difference in standard deviation values obtained for the different sampling frequencies tested. We also observe that the MAS estimator, the UQDE and the estimator searching for the correlation phase root provide roughly the same accuracy for all sampling frequencies.

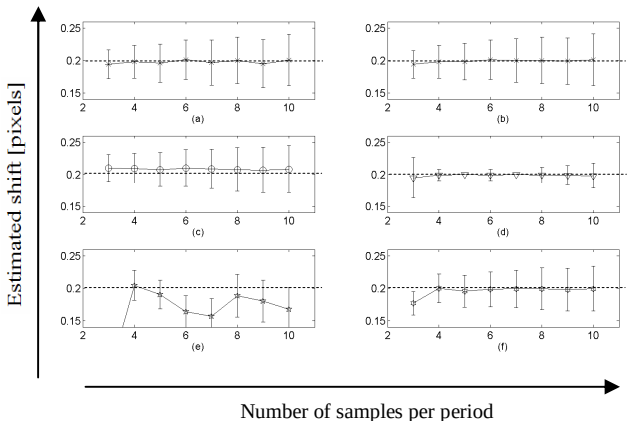

Figure 3. Shift estimations for signals with a SNR of 20dB for different number of samples per period with (a) the MAS estimator (b) the MAS estimator using the unwrapped phase, (c) the complex correlation phase root, (d) the cross-correlation maximum, (e) the quadrature time delay estimator (QDE) and (f) the unbiased quadrature time delay estimator (UQDE). The true shift is 0.2 (dashed line).

VI. Application Results

A. Simulated images

As explained in section IV, the MAS estimator is used for n equal to 2 as the 2-D local translation estimation with block-based motion estimation methods. The application concerns motion tracking with ultrasound images. The performance of the estimator is tested with two simulated images. The formation of the RF simulated images is based on the spatial convolution product over the variables x_1 and x_2 [23].

$$i(x_1,x_2) = h(x_1,x_2) \underset{(x_1,x_2)}{\otimes} m(x_1,x_2), \qquad \textbf{(26)}$$

where i is the radiofrequency image, $h(x_1,x_2)$ is the impulse response of the imaging system, $m(x_1,x_2)$ is a discrete distribution of scatterers representing the medium and $\underset{(x_1,x_2)}{\otimes}$ denotes the spatial convolution over both directions.

In our simulation, h has the following analytic expression:

$$h(x_1,x_2) = \cos(2\pi f_1 x_1)\cos(2\pi f_2 x_2)\exp\left(-\pi\left(\frac{x_1^2}{\sigma_1^2}+\frac{x_2^2}{\sigma_2^2}\right)\right) \qquad \textbf{(27)}$$

For the computer simulation, the values of the parameters were chosen so that they correspond to a possible real ultrasound image formation [13]:

$$f_1 = \frac{1}{1.2}mm^{-1},\ f_2 = \frac{1}{0.2}mm^{-1};\ \sigma_1 = 2mm,\ \sigma_2 = 1mm$$

The simulated medium corresponds to a surrounding 20×30 mm^2 homogeneous medium with a cylindrical inclusion in the center measuring 10 mm in diameter. We considered a spatial Gaussian distribution of the Young modulus. Thus, the central point was set at 100 kPa, twice as hard as the surrounding medium, and the Poisson coefficient was 0.49.

Two ultrasound images were computed to simulate a 2% axial compression of the medium, corresponding to a 0.98% lateral dilatation. The true displacement was obtained using the finite element software tool Femlab (COMSOL AB, Sweden). Initially, the images are simulated with sampling frequencies corresponding to roughly five times the usual ultrasound image resolutions in the axial direction and two times in the lateral direction. Thus, 50 samples per period are simulated on each image direction. Pixel dimension in this case was 3.8×25μm^2. Moreover, both images are decimated on each direction by factors from 2 to 12 by filtering the data with an 8th order Chebyshev lowpass filter. This is done to show the accuracy of our motion estimation method for different sampling frequencies. Its accuracy with low sampled images is an important issue in ultrasound elastography, in the purpose of a real time implementation. As explained above, block-based estimation methods are used to estimate the motion between each image pair obtained previously. Four local estimators are processed. The first one uses the MAS estimator, as explained in Section IV; the second uses the maximum of the cross correlation estimator (MCC). The third method, based on the 1-D complex correlation phase root estimator (CCPR), is presented in [13]. The fourth method tested is the same as in [13], but

with the 1-D UQDE estimator instead of the correlation phase root estimator. For each resolution level and for all four methods, block size was set at two signal periods in both directions. With the MCC estimator, since its accuracy depends directly on image resolution, a search grid linear interpolation (SGI) strategy [2] was employed to compensate for image decimation. Thus, when searching for the best matching block with the cross-correlation cost function, the search zone is interpolated to improve the precision of the local estimation.

The results are compared using the absolute error between the true and estimated displacement vector norms. Figure 4 shows the mean and standard deviation values of the absolute errors for each method versus the decimation factor. The accuracy of the MAS estimator does not depend on image resolution. Thus, we show that even after decimating the images by a factor of 12, which corresponds to signals with four points per period on each direction, the MAS estimator provides the same accuracy as a classical estimator for resolutions that are ten times higher versus the decimation factor. We observe that the accuracy of the MAS estimator does not depend on the images resolution. Thus, we show that even after decimating the images by a factor of 12, which corresponds to normalized frequencies of 1/4 on each direction, the MAS estimator provides the same accuracy as a classical estimator for resolutions that are ten times higher.

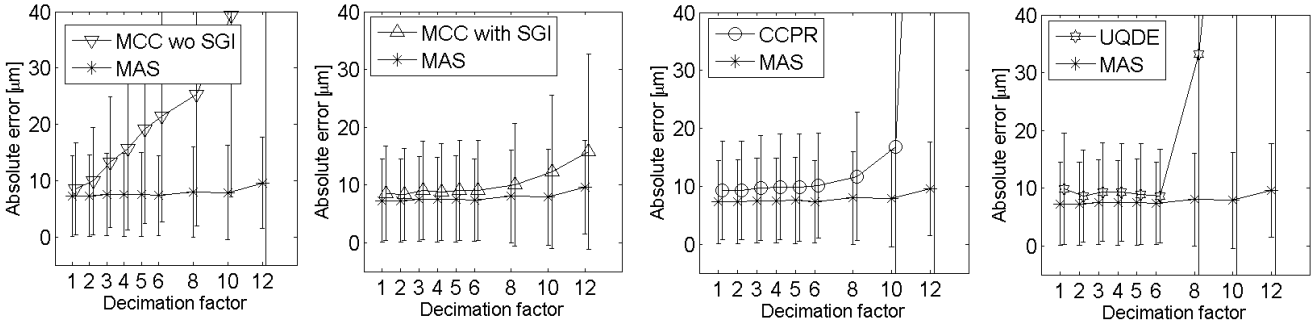

Figure 4. Comparison of mean and standard deviation values of the absolute error between the true and estimated vector norms with the original and decimated images between MAS estimator and (a) maximum cross-correlation estimator without search grid interpolation, (b) maximum correlation estimator with search grid interpolation, (c) complex correlation phase zero crossing estimator, and (d) unbiased quadrature delay estimator.

Figure 4 shows that the MCC estimator gives a minimum error of roughly 8 µm (which corresponds to a relative error of 0.3%) for images at the initial resolution. For the initial resolution level, the MAS estimator provides less error and reaches the value of 8 µm when the resolution level is divided by 10. Therefore, a resolution that is 10 times higher is needed for the MCC estimator reported to the MAS phase estimator. In this case of equivalent accuracies, the computation time using the MCC estimator is 14 times longer than the computation time with the proposed estimator. Note in Figures 4(c) and (d) that for all resolution levels the methods using CCPR and UQDE produce an absolute error higher than the MAS estimator. This may be explained by several reasons. First, the 1-D formulation of CCPR and UQDE estimators is not well adapted to estimate 2-D displacements. Moreover, UQDE uses the signals amplitude, which makes it less efficient in speckle imaging applications (as is the case of ultrasound imaging) than estimators using the phase [11]. The motion initialization used here for each node [21] may also not be adapted for these 1-D estimators. Thus, an estimation error that can occur for one node is propagated for the neighboring nodes and increases the total amount of error. This can be the case especially for UQDE, which is more sensitive to speckle changes than CCPR. For these reasons, only the CCPR method is retained for the experimental case.

B. Experimental images

The experimental result presented here is considered with phantom data. The phantom (Elasticity QA Phantom, model 049, by CIRS Tissue Simulation & Phantom Technology, Norfolk, VA, USA) was designed for ultrasound elastography and presented a spherical 20-mm-diameter inclusion of 6 kPa for a surrounding medium of 29 kPa. The ultrasound RF images were acquired and formed using the beamforming method presented by Liebgott et al. in [13]. Two images for two different compression levels were acquired, with 8 points per period in the axial direction and 24 in the lateral direction, corresponding to a pixel size of 19.6×75.2 µm2. The compression of the phantom was directly applied with the ultrasound probe, as with freehand elastography for clinical applications [21]. The same motion estimation methods used with the simulated images were considered. MAS, MCC and CCPR estimators were tested. For the experimental data, since the true displacement was not available, a confidence measure was used to quantify the estimation accuracy. We therefore applied the estimated 2-D displacement to image i_2 in order to map it onto the reference image i1. Furthermore, we calculated the 2-D normalized cross-correlation coefficient between each block considered on i_1 and its corresponding block on the registered version of i_2. The similarity measure, denoted ξ, is then the mean value of all these coefficients.

Figure 5(a) shows the evolution of ξ and of the standard deviation values of ξ for the three methods when original images are decimated. Figure 5(b) compares the accuracy of the MAS estimator to the MCC estimator with the search grids refined for different interpolation factors and using the original images.

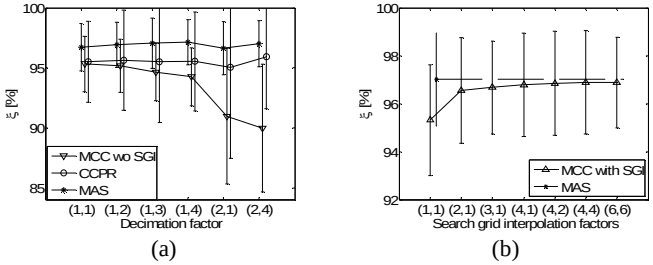

Figure 5. Accuracy measurement (a) using the MAS, MCC or CCPR local estimator for different decimation factors (axial, lateral), (b)

with the MCC using the original images and the search grid refine for different interpolation factors (axial, lateral)

The results of comparing MAS and MCC with the original images and MCC with the search grids interpolated by a factor of 6 in each direction are given in figure 6. The estimated motion vectors for a region around the inclusion are shown, as well as the ultrasound image. Thus, for roughly the same computation time (Figure 6 (b) and (c)) the estimation accuracy with the MAS estimator is much higher than with the classical MCC. To reach the same accuracy level with MCC, search grids must be linearly interpolated by a factor of 6 in both directions. Note that this method of searching for the best matching block with the MCC refines the precision of the local motion estimation with no increase in the computation complexity of the cross-correlation. However, the computation time in this case becomes roughly ten times higher than with the MAS estimator on the original images.

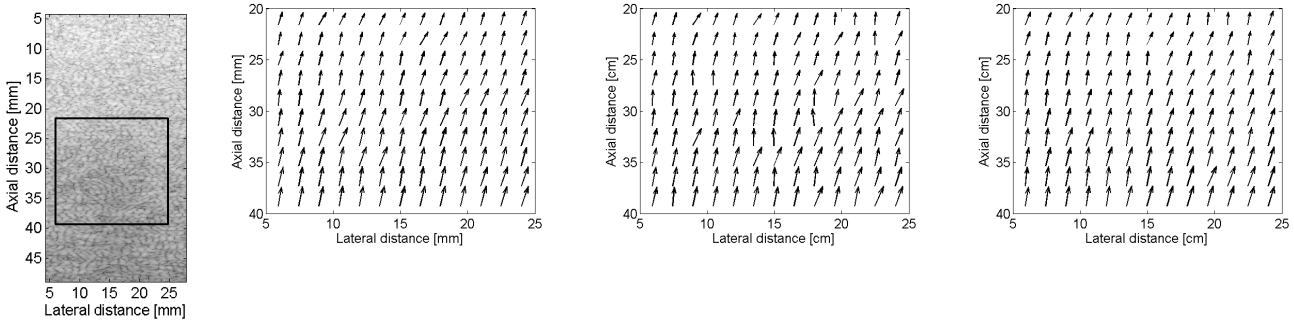

(a) (b) (c) (d)

Figure 6. (a) Ultrasound image and estimated 2-D motion vectors corresponding to the region designated by the rectangle on the ultrasound image, estimated using (b) MAS, (c) MCC, (d) MCC with SGI and an interpolation factor of 6 in each direction.

VII. CONCLUSIONS

An analytic subsample spatial shift estimation method is proposed. The estimation is based on an a priori form of n-D signals based on a nonconventional technique of forming ultrasound images. A series of analytic signals is generated and shown to present linear phases with respect to all directions. Thus, a linear estimation problem is obtained. The choice of n particular complex signals allows us to analytically solve the linear system and consequently to provide an analytic estimation. The simulation results show the performance of the proposed estimator for subsample estimation and its accuracy for low sampled signals compared to classical methods.

For two dimensions, we showed how the proposed estimator can be used for motion tracking with block-based motion estimation methods. The proposed estimator is then shown to perform better than the classical maximum of the cross-correlation estimator, an estimator dedicated to ultrasound elastography that searches for the root of the complex correlation phase and an estimator using the in-phase and quadrature-phase components of signals.

As one of the major problems in motion estimation for ultrasound elastography is the out-of-plane displacements, the three-dimensional case will be considered in a future study. The n-D formulation of the analytic estimator in this case makes it possible to directly estimate the three components of the local tissue displacement vector. Moreover, its accuracy for low sampled signals is also relevant to the 3-D case to reduce the amount of processed data.

APPENDIX

We use the induction method to show that the phases of the analytic signals defined in (5) follow the linear model in (7) for any integer *n*. Let us note the result which is to be proved here by *E*(*n*).

$$E(n):\ \phi_i(\mathbf{x}) = \sum_{k=1}^{n} 2\pi f_k (-1)^{b_{ik}} (x_k - d_k) \tag{28}$$

We start by checking the basis step *E*(*1*).

Case n = 1:

$$\begin{aligned} R_i(u_1) &= R(u_1)\left(1+(-1)^{b_{i1}}\operatorname{sign}(u_1)\right) \\ &= R(u_1) + j(-1)^{b_{i1}} R_H(u_1) \end{aligned} \tag{29}$$

With the signal model in (1) and assuming the disjointed Fourier spectrum between the window $w(x_1)$ and the 1-D cosinus, the analytic signal defined in (29) becomes:

$$\begin{aligned} & r_i(x_1) \\ &= w(x_1)\left(\cos\left(2\pi f_1(x_1-d_1)\right) + j(-1)^{b_{i1}} \sin\left(2\pi f_1(x_1-d_1)\right)\right) \\ &= w(x_1)\exp\left(j2\pi f_1(-1)^{b_{i1}}(x_1-d_1)\right) \end{aligned} \tag{30}$$

From this it can easily be concluded that *E*(*1*) is true.

We assume now that *E*(*n*) is true (inductive hypothesis) and we need to show that *E*(*n+1*) is true.

Case $E(n)$ *true* $\Rightarrow E(n+1)$ *true*

Considering *E*(*n*) true and keeping in mind the separable form of the cosinus product, the analytic signal r_i for the case *n+1* can be written as follows:

$$
\begin{aligned}
& r_i(\boldsymbol{x}) = w(\boldsymbol{x}) exp\left(j \sum_{k=1}^{n} 2\pi f_k (-1)^{b_k} (x_k - d_k) \right) \times \\
& \left[cos\left(2\pi f_{n+1} (x_{n+1} - d_{n+1})\right) + j(-1)^{b_{n+1}} sin\left(2\pi f_{n+1} (x_{n+1} - d_{n+1})\right) \right] \qquad \textbf{(31)} \\
& = w(\boldsymbol{x}) exp\left(j \sum_{k=1}^{n} 2\pi f_k (-1)^{b_k} (x_k - d_k) \right) \times \\
& exp\left(j\, 2\pi f_{n+1} (-1)^{b_{n+1}} (x_{n+1} - d_{n+1}) \right) \\
& = w(\boldsymbol{x}) exp\left(j \sum_{k=1}^{n+1} 2\pi f_k (-1)^{b_k} (x_k - d_k) \right)
\end{aligned}
$$

In (31) we show that $E(n+1)$ is also true. Thus, the conditions of the induction method are met and we conclude that $E(n)$ is true for all integers n.

REFERENCES

[1] Ophir, J., Césepedes, I., Ponnekanti, H., Yazdi, Y. and Li, X., Elastography: a quantitative method for imaging the elasticity of bilogical tissues, *Ultrasonic Imaging*, vol.13, pp. 111-134, 1991.

[2] Giachetti, A., Matching techniques to compute image motion, *Image vision and computing*, pp. 247-260, 2000.

[3] Wiegand, T., Sullivan, G. J., Bjontegaard, G., Luthra, A., Overview of the H.264/AVC video coding standard, *IEEE Transactions on Circuits and Systems for Video Technology*, 2003, vol. 13, n°7, 560-576.

[4] Zhang, X., Ai, H., Hu, R., Li, D., A novel algorithm for sub-pixel block motion estimation, *International Symposium on Intelligent Multimedia, Video and Speech Processing*, 2004.

[5] Giunta, G., Fine estimators of two-dimensional parameters and application to spatial shift estimation, *IEEE Transactions on Signal Processing*, vol. 47, no.12, 1999.

[6] Dufaux, F., Moscheni, F., Motion estimation techniques for digital TV: A review and a new contribution, Proceedings of IEEE, 1995, Vol.83, No.6, p. 858-876.

[7] So, H.C., A comparative study of two discret-time phase delay estimators, *IEEE Transactions on Instrumentation and Measurement*, vol.54, no.6, pp. 2501-2504, 2005.

[8] Maskell, D. L., Woods, G. S., The discrete-time quadrature subsample estimation of delay, *IEEE Transactions on Instrumentation and Measurement*, vol.51, no.1, pp. 133-137, 2002.

[9] Pinton, G., Dahl, J., and Trahey, G., Rapid tracking of small displacements with ultrasound, *IEEE ultrasonics, ferroelectrics, frequency control*, vol. 53, pp. 1103–1118, 2006.

[10] Pesavento A., Perrey, C., Krueger, M. and Ermert, H., A time-efficient and accurate strain estimation concept for ultrasonic elastography using iterative phase zero estimation, *IEEE ultrasonics, ferroelectrics, and frequency control*, vol. 46(5), pp. 1057-1067, 1999.

[11] Ebbini, E. S., Phase-coupled two-dimensional speckle tracking algorithm, *IEEE Transactions on Ultrasonics, Ferroelectrics, and Frequency Control*, 53(5): pp. 972-990,2006.

[12] Jensen, J. A., A new method for estimation of velocity vectors, *IEEE ultrasonics, ferroelectrics, frequency control*, vol. 45, pp. 837–851, 1998.

[13] Liebgott, H., Wilhjelm, J.E., Jensen, J.A., Vray, D. and Delachartre, P., PSF dedicated to estimation of displacement vectors for tissue elasticity imaging with ultrasound, *IEEE ultrasonics, ferroelectrics, and frequency control*, vol. 54(4), pp. 746-756, 2007.

[14] Boashash, B., Estimating and interpreting the instantaneous frequency of a signal - Part 1: Fundamentals. *Proceedings IEEE*, vol. 80, pp. 520 - 538, 1992.

[15] [15] Hahn, S.L., *Hilbert Transforms in Signal Processing*: Boston, MA: Artech House. 1996.

[16] [16] T. Bullow, Sommer, G., Hypercomplex Signals—A novel extension of the analytic signal to the multidimensional case, *IEEE Transactions on Image Processing*, vol.49, no.11, 2001.

[17] [17] Eldar, Y.C. and Oppenheim, A.V., Covariance shaping least-squares estimation. *IEEE Transactions on Signal Processing*, vol. 51(3): pp. 686-697, 2003.

[18] de Coulon, F., *Signal theory and processing*: Artech House, Dedham, Massachusetts. 1986.

[19] Kay, S. and Nekovei, R., An efficient two-dimensional frequency estimator. *IEEE Trans. Acoust., Speech, Signal Processing*, vol. 38(10), pp. 1807 - 1810, 1990.

[20] Tretter, S., Estimating the frequency of a noisy sinusoid by linear regression (Corresp.). *IEEE Transactions on Information Theory*, vol. 31(6), pp. 832-835, 1985.

[21] Basarab, A., Liebgott, H., Morestin, F., Lyshchik, A., Higashi, T., Asato, R., Delachartre, P., A method for vector displacement estimation with ultrasound images and its application for thyroid nodular disease, *Medical Image Analysis*, vol. 12(3), pp. 259 - 274, 2008

[22] Zhang, L., Wu, W., On the application of cross-correlation function to subsample discrete time delay estimation, *Digital Signal Processing*, vol.16, pp. 682-694, 2006.

[23] Yu, Y., Acton, S. T., Speckle reducing anisotropic diffusion, *IEEE Transactions on Image Processing*, 2002, vol. 11, n°11, 1260-1270.